Self-assembly of magnetic Janus colloids with radially shifted dipoles under an external magnetic field

Jonathan A. Victoria-Camacho,[1] Ubaldo M. Córdova-Figueroa,[2]
[1] Department of Bioengineering, University of Puerto Rico–Mayagüez, Mayagüez, PR 00681, USA
[2] Department of Chemical Engineering, University of Puerto Rico–Mayagüez, Mayagüez, PR 00681, USA

1. Comparison of Sample Sizes: $N = 500$ vs. $N = 1000$

In order to evaluate the statistical robustness of the results, we compared the simulations performed with $N = 500$ and $N = 1000$ particles for $\alpha = 10$ and $\alpha = 100$. The analysis includes the nucleation process, and the power-law behavior of the corresponding observables. Overall, no significant differences were observed between the two sample sizes, indicating that the system already reaches statistical convergence for $N = 500$. The nucleation dynamics and steady-state structures remain consistent, as do the scaling exponents obtained from the power-law fits. Similarly, the orientation distributions for both values of α show negligible variations, confirming that the global alignment properties are not sensitive to the number of simulated particles within this range.

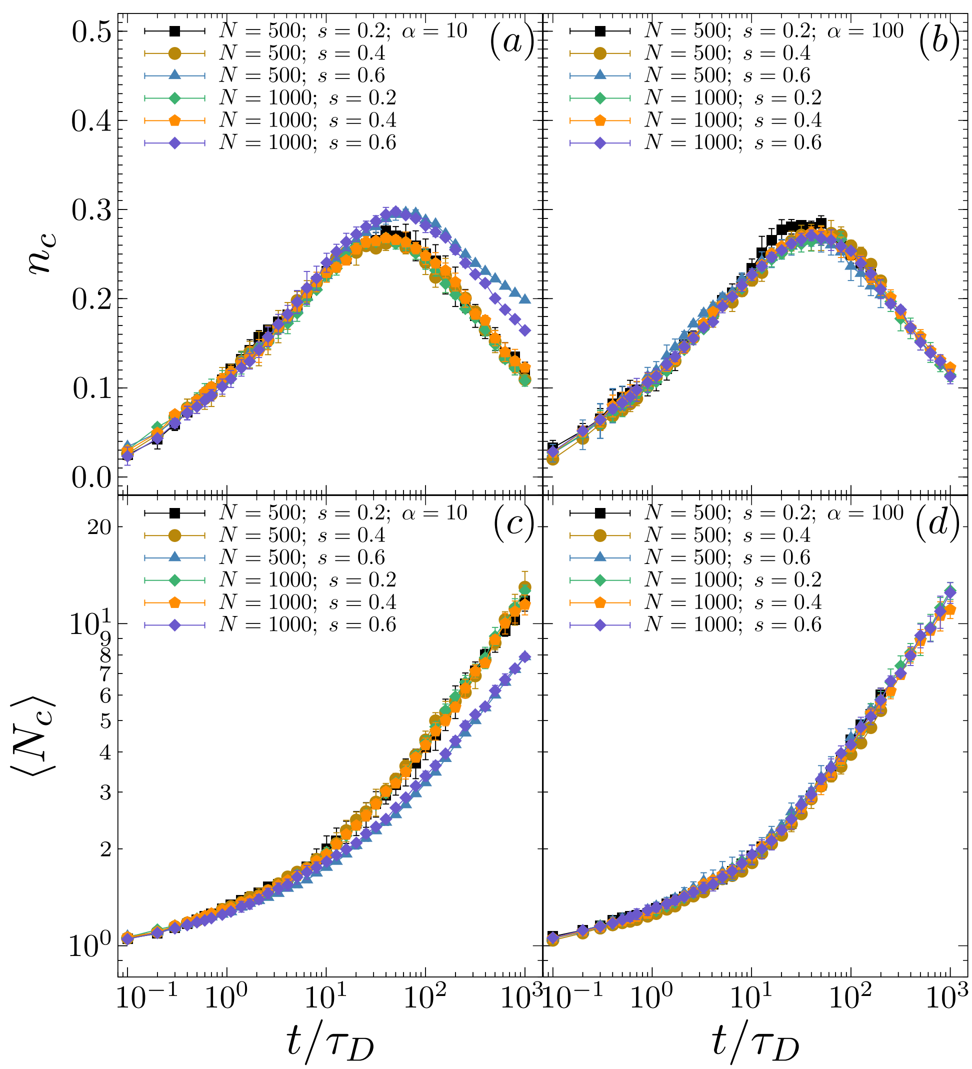

Figure S1: Comparison between simulations with $N = 500$ and $N = 1000$ particles for $\alpha = 10$ and $\alpha = 100$. (a) Nucleation for $\alpha = 10$; (b) Nucleation for $\alpha = 100$; (c) Power-law behavior for $\alpha = 10$; (d) Power-law behavior for $\alpha = 100$; No significant differences are observed between both sample sizes, indicating convergence of the statistical properties.

2. Extrapolated values for the average dipolar alignment

Figure S2 shows the extrapolated values for the average dipolar alignment $(\mathbf{m}_i \cdot \mathbf{m}_j)_{\text{med}} / m^2$ (S2 (a)) and the growth exponent z (S2 (b)) for $s > 0.75$. The initial values for $\alpha = 0$ correspond to those reported by Victoria-Camacho et al. (2020), where the self-assembly of magnetic Janus particles (MJPs) with axially shifted dipoles in absence of a magnetic field was analyzed. This theoretical extrapolation enables us to predict the behavior of aggregates when the dipole is located near the particle surface. The approach considers the magnetic interaction potential between the dipoles of two neighboring particles. Analysis of the potential reveals that the system's minimum energy state for $s \geq 0.8$ is located at $(\mathbf{m}_i \cdot \mathbf{m}_j) / m^2 = 1$, indicating that the magnetic potential is nearly identical across such systems. Thus, the extrapolated data support the observed magnetic alignment tendency in high-shift regimes.

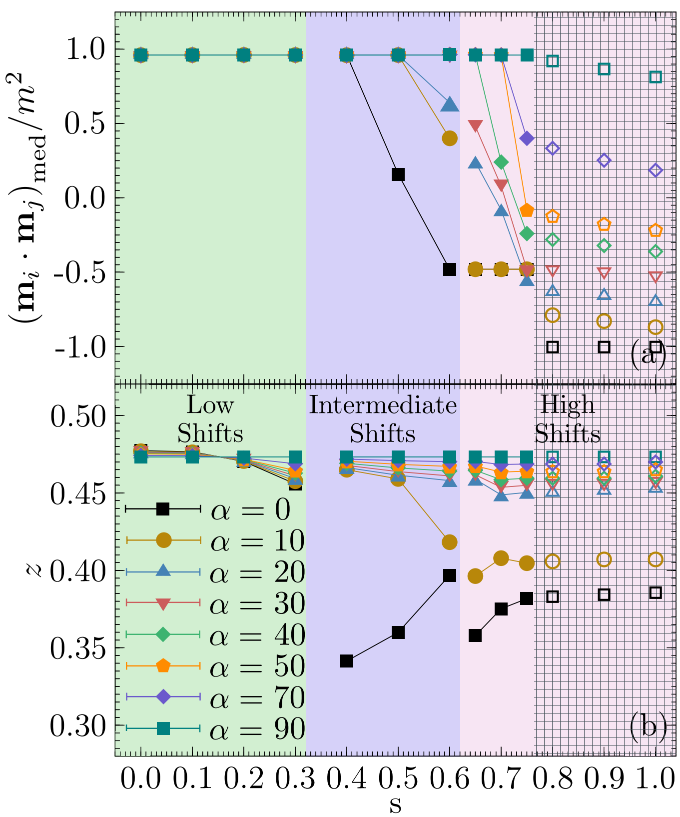

Figure S2: Extrapolated values of the average dipolar alignment $(\mathbf{m}_i \cdot \mathbf{m}_j)_{\text{med}} / \|\mathbf{m}\|^2$ (a) and the cluster growth exponent z (b) for various dipole shifts s and field strengths α. Results for $\alpha = 0$ are consistent with previously reported values for axially shifted dipoles in absence of a magnetic field. Section with mesh indicates extrapolated region, and open points indicate extrapolated values.

3. Derivation of the Magnetic Ratio R_{Mag}

The magnetic ratio R_{Mag} is defined as the competition between the torque induced by the external field, which aligns the dipoles (T^H), and the reconstructive torque due to dipole–dipole interactions (T^P):

$$R_{Mag} = \frac{T^H}{T^P}. \tag{1}$$

The reconstructive torque can be expressed as the sum of a force–torque coupling term and a direct dipolar torque,

$$T^P = as\,\frac{3\mu_0 m^2}{4\pi r_{d_{ij}}^4} + \frac{\mu_0 m^2}{4\pi r_{d_{ij}}^3},$$

where s is the reduced dipolar shift. The torque from the external field is simply

$$T^H = \mu_0 m H.$$

Introducing the dimensionless dipolar coupling constant,

$$\lambda = \frac{\mu_0 m^2}{4\pi a^3 kT},$$

and the Langevin parameter,

$$\alpha = \frac{\mu_0 m H}{kT},$$

together with the dimensionless center-to-center distance between neighboring dipoles $r^*_{dij} = r_{dij}/a$, the ratio becomes

$$R_{Mag} = \frac{\mu_0 m H}{as\frac{3\mu_0 m^2}{4\pi}\frac{1}{r_{d_{ij}}^4} + \frac{\mu_0 m^2}{4\pi}\frac{1}{r_{d_{ij}}^3}}$$

By inserting a dimensionless factors $\frac{1}{a^3/a^3}$ and $\frac{1/kT}{1/kT}$, one obtains

$$R_{Mag} = \frac{\frac{\mu_0 m H}{kT}}{s\frac{3\mu_0 m^2}{4\pi a^3 kT}\frac{a^4}{r_{d_{ij}}^4} + \frac{\mu_0 m^2}{4\pi a^3 kT}\frac{a^3}{r_{d_{ij}}^3}}$$

$$R_{Mag} = \frac{\alpha}{\lambda\left(\frac{3s}{(r^*_{dij})^4} + \frac{1}{(r^*_{dij})^3}\right)}.$$

Finally, multiplying numerator and denominator by $(r^*_{dij})^3$ yields the compact form

$$R_{Mag} = \frac{(r^*_{dij})^3\,\alpha}{\lambda\left(1 + s\frac{3}{r^*_{dij}}\right)}. \tag{2}$$

This nondimensional expression highlights the competition between field-induced alignment (via α) and dipole–dipole reconstruction (via λ and s).

4. Magnetic ratio R_{Mag}

Figure S3 shows the magnetic ratio R_{Mag} as a function of the field strength α for different dipolar shifts s, using two approaches to estimate the dipole-dipole distance r^*_{dij}. In S3(a), r^*_{dij} is computed based on the average alignment $(\mathbf{m}_i \cdot \mathbf{m}_j)/\|\mathbf{m}\|^2$ from Figure S2. This plot demonstrates that R_{Mag} exhibits exponential growth for $\alpha > 10^2$, approaching the behavior expected when $r^*_{dij} = 2$. This is attributed to strong magnetic fields that align the dipoles fully along the field direction, effectively making $(\mathbf{m}_i \cdot \mathbf{m}_j)/\|\mathbf{m}\|^2 \approx 1$. In contrast, S3(b) shows the same relationship assuming a constant $r^*_{dij} = 2$. In both cases, the critical threshold $R_{\mathrm{Mag}} = 1$ indicates the balance between the dipole-dipole interaction torque and the field-induced alignment torque. For $R_{\mathrm{Mag}} < 1$, the system is dominated by dipolar interactions, while $R_{\mathrm{Mag}} > 1$ indicates field-dominated alignment. In particular, the critical value of α for which $R_{\mathrm{Mag}} = 1$ depends on how r^*_{dij} is computed for $s > 0.5$, whereas for $s \leq 0.5$ the result is largely insensitive to this choice. This explains the abrupt morphological transition from unaligned aggregates to field-aligned chains observed for $s \leq 0.5$, and the existence of an intermediate region with chiral clusters for $s > 0.5$, where dipolar interactions still resist full alignment despite the external field.

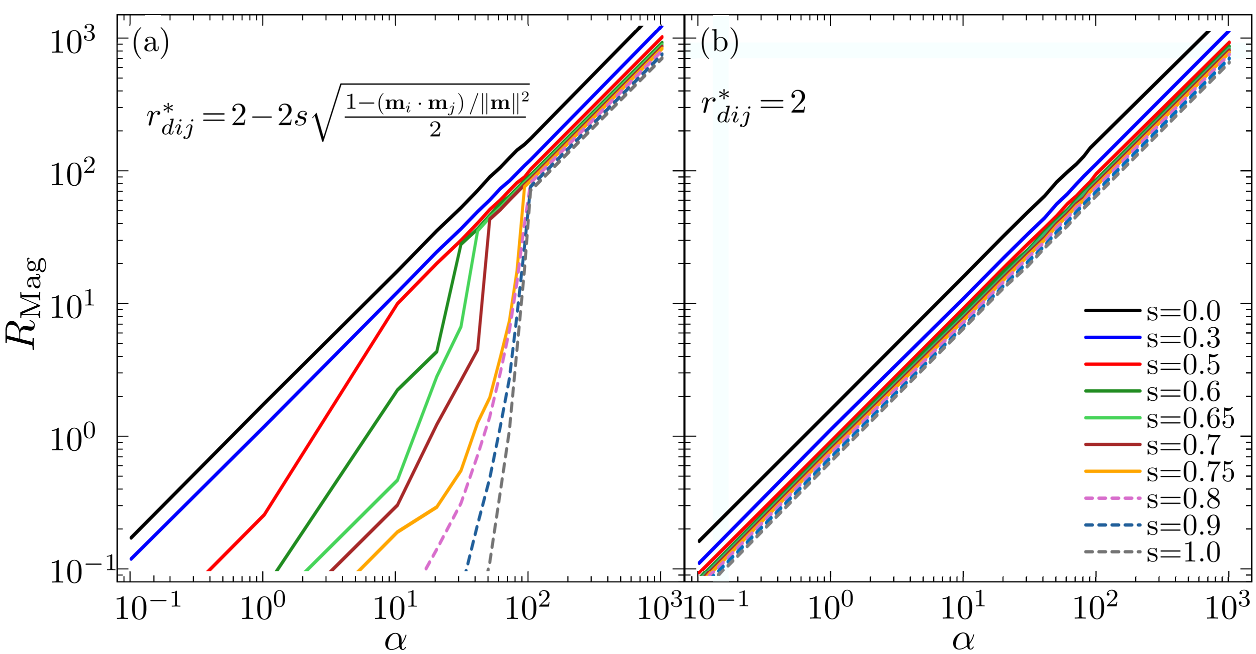

Figure S3: (a) Magnetic ratio R_{Mag} as a function of field strength α for $\lambda = 45$, using the computed distance $r^*_{dij} = 2 - 2s\sqrt{(1 - (\mathbf{m}_i \cdot \mathbf{m}_j)/\|\mathbf{m}\|^2)/2}$. (b) Magnetic ratio R_{Mag} as a function of field strength α for $\lambda = 45$, assuming fixed $r^*_{dij} = 2$. Solid lines indicate values calculated by simulation, dashed lines indicate extrapolated values.

5. Videos

The following videos are provided in the file `Videos.zip`:

- `alpha00s03.mov`
  Video of the dynamic simulation for $\lambda = 45$, $\alpha = 00$, and $s = 0.3$.
- `alpha00s05.mov`
  Video of the dynamic simulation for $\lambda = 45$, $\alpha = 00$, and $s = 0.5$.
- `alpha00s07.mov`
  Video of the dynamic simulation for $\lambda = 45$, $\alpha = 00$, and $s = 0.7$.
- `alpha40s03.mov`
  Video of the dynamic simulation for $\lambda = 45$, $\alpha = 40$, and $s = 0.3$.
- `alpha40s05.mov`
  Video of the dynamic simulation for $\lambda = 45$, $\alpha = 40$, and $s = 0.5$.
- `alpha40s07.mov`
  Video of the dynamic simulation for $\lambda = 45$, $\alpha = 40$, and $s = 0.7$.
- `alpha90s03.mov`
  Video of the dynamic simulation for $\lambda = 45$, $\alpha = 90$, and $s = 0.3$.
- `alpha90s05.mov`
  Video of the dynamic simulation for $\lambda = 45$, $\alpha = 90$, and $s = 0.5$.
- `alpha90s07.mov`
  Video of the dynamic simulation for $\lambda = 45$, $\alpha = 90$, and $s = 0.7$.